AUTHOR QUERY FORM

ELSEVIER	**Journal: SOSI** **Article Number: 13055**	**Please e-mail or fax your responses and any corrections to:** **Roshan, Sajeev** **E-mail: Corrections.ESCH@elsevier.spitech.com** **Fax: +1 619 699 6721**

Dear Author,

Please check your proof carefully and mark all corrections at the appropriate place in the proof (e.g., by using on-screen annotation in the PDF file) or compile them in a separate list. Note: if you opt to annotate the file with software other than Adobe Reader then please also highlight the appropriate place in the PDF file. To ensure fast publication of your paper please return your corrections within 48 hours.

For correction or revision of any artwork, please consult http://www.elsevier.com/artworkinstructions.

Any queries or remarks that have arisen during the processing of your manuscript are listed below and highlighted by flags in the proof. Click on the 'Q' link to go to the location in the proof.

Location in article	Query / Remark: click on the Q link to go Please insert your reply or correction at the corresponding line in the proof
Q1	Please confirm that given names and surnames have been identified correctly.
Q2	Two sets of captions have been provided for Figs. 1-10. Please check if the captured captions are correct, and amend as necessary.
Q3	Two sets of captions have been provided for Tables 1 and 2. Please check if the captured captions are correct, and amend as necessary.
Q4, Q5, Q6, Q7, Q8, Q9	This sentence has been slightly modified for clarity. Please check that the meaning is still correct, and amend if necessary.
Q10	This sentence has been reworded for clarity. Please check that the meaning is still correct. Please check this box if you have no corrections to make to the PDF file. ☐

Thank you for your assistance.

Solid State Ionics xxx (2013) xxx

Contents lists available at ScienceDirect

Solid State Ionics

journal homepage: www.elsevier.com/locate/ssi

Highlights

Solid State Ionics xxx (2013) xxx–xxx

Electrical properties of the $(Y_{2-x}Li_x)Ti_2O_{7-x}$ samples with $LiO_{0.5}$ self-flux

L.C. Wen [a], Y.I. Tsai [a], H.K. Lin [a], S.C. Chang [a], M.Y. Lin [a], H.S. Chang [a], H.-C.I. Kao [a,*], L.Y. Jang [b], M.C. Lee [c], Y.S. Lee [c]

[a] Department of Chemistry, Tamkang University, Tamsui 25137, Taiwan
[b] National Synchrotron Radiation Research Center, Hsinchu 30076, Taiwan
[c] Institute of Nuclear Energy Research, Atomic Energy Council, Longtan 32546, Taiwan

- Co-existence of flux with YLT $(Y_{2-x}Li_x)Ti_2O_{7-x}$, conductivity was not affected
- Addition of $LiO_{0.5}$ as a flux in the YLT, preparation temperature was lowered
- For $x = 0.070$, which has the highest σ (total) and the lowest activation energy
- Ti atoms are in the mixed valence state.
- At 500 °C, no electronic conductivity is observed.

0167-2738/$ – see front matter © 2013 Published by Elsevier B.V.
http://dx.doi.org/10.1016/j.ssi.2013.09.034

Solid State Ionics xxx (2013) xxx–xxx

Contents lists available at ScienceDirect

Solid State Ionics

journal homepage: www.elsevier.com/locate/ssi

Electrical properties of the $(Y_{2-x}Li_x)Ti_2O_{7-x}$ samples with $LiO_{0.5}$ self-flux

L.C. Wen [a], Y.I. Tsai [a], H.K. Lin [a], S.C. Chang [a], M.Y. Lin [a], H.S. Chang [a], H.-C.I. Kao [a,*], L.Y. Jang [b], M.C. Lee [c], Y.S. Lee [c]

[a] Department of Chemistry, Tamkang University, Tamsui 25137, Taiwan
[b] National Synchrotron Radiation Research Center, Hsinchu 30076, Taiwan
[c] Institute of Nuclear Energy Research, Atomic Energy Council, Longtan 32546, Taiwan

ARTICLE INFO

Article history:
Received 11 February 2013
Received in revised form 21 September 2013
Accepted 22 September 2013
Available online xxxx

Keywords:
Pyrochlore
Titanate
Flux
Electrical property
Oxide ion conductor

ABSTRACT

A series of $(Y_{2-x}Li_x)Ti_2O_{7-x}$ samples abbreviated as YLT-2L were prepared by the addition of 2*x* moles of $LiO_{0.5}$ self-flux into the parent compound, where $x = 0.040$ to 0.110. Preparation temperatures were either 1300 or 1350 °C, depending on the amount of flux addition. However, the $Y_2Ti_2O_7$ had no $LiO_{0.5}$ co-existence; it was prepared at the highest temperature, 1600 °C. Relative densities of all the YLT-2L samples were larger than 97%, but for the $Y_2Ti_2O_7$, it was 94.3(2)% only. By the addition of flux, preparation temperature reduced for more than 250 °C. Among all the YLT-2L samples, the one with $x = 0.070$ had the highest total electrical conductivity $(2.90(2) \times 10^{-4}\ S \cdot cm^{-1}$ at 700 °C) and the lowest total activation energy (0.99(1) eV). By doping Li ion into the Y-site, oxygen vacancies were created, although YLT-2L samples had flux co-existence, electrical conductivity was still comparable to the parent compound reported by Yamaguchi et al. (1998) and Kobayashi et al. (2002). At 500, 600 and 700 °C, the ionic transference numbers (t_i) found for the YLT-2L samples were 1.00(2), 0.96(2) and 0.90(3), respectively, and did not vary with the amount of substitution and the flux addition. Contribution of the electronic conductivity was due to the presence of a small amount of the Ti^{3+} ions in the samples investigated by the Ti *K*-edge XANES spectra.

1. Introduction

Solid oxide fuel cells (SOFCs) have been developed rapidly in recent years due to their all solid state components which let the application region become broadened. SOFC is a highly efficient power generation system due to its several advantages, such as high energy conversion efficiency, fuel flexibility and reduced pollution [1,2]. In general, SOFC framework is based on a sandwiched structure, including a dense electrolyte, such as YSZ [3], between two porous electrodes, which are Ni-YSZ [4] for the anode and $La_{1-x}Sr_xMnO_3$ [5] for the cathode.

Solid oxide ionic conductors with a pyrochlore phase ($A_2B_2O_7$) gain considerable attention because of their similar structure with the YSZ (yttria stabilized zirconia) which is a commercialized material used in the SOFC [3] and oxygen sensor [6]. YSZ has a fluorite phase [7] and pyrochlore phase is a superstructure of the fluorite [8]. For a pyrochlore phase, the occupancy factor (OF) of the 8*b* site ranges from 0 to less than 0.875 depending on the ordering of the unit cell. A complete ordered pyrochlore unit cell has an empty 8*b* site. For a disordered pyrochlore, the 8*b* site is partially occupied [9–11]. Yamamura et al. studied a series of $R_2Zr_2O_7$ and found that $Gd_2Zr_2O_7$ was on the phase change boundary. For a smaller R, $R_2Zr_2O_7$ had a fluorite phase. For an R ion bigger than Gd, $R_2Zr_2O_7$ has a pyrochlore phase. Among them, $Eu_2Zr_2O_7$ had the highest electrical conductivity [12] and it had a disordered pyrochlore phase. Around the phase change boundary, on the pyrochlore side, electrical conductivity is greatly enhanced. Nevertheless, it decreased while pyrochlore phase becomes more ordered so that electrical conductivity depends on the ordering of the pyrochlore phase and the crystalline phase of the $R_2Zr_2O_7$ is dependent on the ionic radius ratio of the r_R to r_{Zr} [12].

In order to have dense solid electrolyte, high sintering temperature (>1600 °C) is usually used in preparation. $Ln_2(Zr,M)_2O_7$ (Ln = La, Nd, Sm, Gd and Er; M = Y, Ti, In and Mg) was sintered at 1650 °C and it has a relative density higher than 95% [13]. $Lu_2Ti_2O_7$ was sintered at 1700 °C for 10 h to achieve 92.5% or 93% dense ceramics [14]. Relative density of the electrolyte affects the electrical conductivity directly [15]. Relative density of the $(Gd_{0.2}Ce_{0.8})O_{1.9}$ prepared by Ivanov et al. with sintering temperatures, 1100–1300 °C, is 94–100%. The sample with lower relative density has lower electrical conductivity and higher activation energy [15]. Lee et al. used $Sr_2Ga_2O_5$ as a sintering aid to prepare the SDC (Sm doped CeO_2) at 1250 °C, electrical conductivity was increased. SDC with 0.5 mol% $Sr_2Ga_2O_5$ had a relative density of 97% and an electrical conductivity of $3.16 \times 10^{-3}\ S \cdot cm^{-1}$ at 450 °C which is higher than the pure SDC with a relative density of 70% and a conductivity of $3.19 \times 10^{-5}\ S \cdot cm^{-1}$ [16].

* Corresponding author at: 151 Ying-chuan Road, Department of Chemistry, Tamkang University, Tamsui, New Taipei City 25137, Taiwan. Tel.: +886 2 2625 1661; fax: +886 2 2620 9924.
E-mail address: kaohci@mail.tku.edu.tw (H.-C.I. Kao).

0167-2738/$ – see front matter © 2013 Published by Elsevier B.V.
http://dx.doi.org/10.1016/j.ssi.2013.09.034

The $Y_2Ti_2O_7$ sample reported by Yamaguchi et al. [17] and Kobayashi et al. [18] had an ionic conductivity of 2.30×10^{-4} and 10^{-4} S·cm^{-1}, respectively. Both of the groups prepared the sample at 1600 °C for 10 h. In our previous report, a series of $(Y_{2-x}Li_x)Ti_2O_{7-x}$ was prepared at 1150 °C. $LiO_{0.5}$ was added as a self-flux to lower the processing temperature and to increase the relative density of the samples. Relative density reached to 97.0(2)% for the $x = 0.100$ sample [19]. In this report, sintering temperature was raised to 1300 °C to obtain fully dense (over 98%) specimens for electrical property measurement and EMF (electromotive force) studies. Valence of the Ti atom was analyzed by the Ti *K*-edge XANES spectra.

2. Experimental

The preparation details of the YLT-2L samples had been reported in our previous paper [19]. The only difference was the sintering temperatures. For the YLT-2L samples, 1300–1350 °C was employed, but for the$Y_2Ti_2O_7$, 1600 °C was used in order to make dense enough samples. Weight percent of the $LiO_{0.5}$ was between 0.31 and 0.87 wt.% when x varied from 0.040 to 0.110, respectively. That is listed in Table 1. Relative density of the sintered specimens was measured by the Archimedes method using de-ionized water as a liquid medium, and morphology of the samples was observed by a VEGA\\SBH scanning electron microscope.

The electrical parameters were determined by the AC impedance spectroscopy (EIS) using the fully automated Autolab PGSTAT30 potentiostat/galvanostat system in air in a frequency range of 1 MHz to 1 Hz and an excitation amplitude of 50 mV. A two-probe method was used for the electrical conductivity measurement. Silver paste was first brushed onto both sides of a disk with ea. 0.9 to 1.1 cm diameter and 0.12 to 0.18 cm thickness. After drying in the oven for 1 h at 700 °C, Pt wires were then attached on the silver layers with silver paste and dried again. The whole set was placed in an oven. An R-type thermocouple was placed near the sample and did the measurement from 500 to 700 °C.

Electrical conductivity with respect to the partial pressure of oxygen was also measured by EIS. Appropriate amount of the oxygen and argon was allowed to flow into the sample chamber to control the oxygen partial pressure. The percentage of the oxygen partial pressure varied from 10% to 100%. The flow rates were fixed by a mass flow controller to a total rate of 100 sccm [20]. The electromotive forces (EMFs) were measured on an oxygen concentration cell, in which ambient air was employed as a reference to one side of the sample, and a mixed gas (ea. 75–85% oxygen and 25–15% argon) was introduced to another side of the cell. The whole system was allowed to stabilize under each condition before the measurement. The theoretical potential was calculated by the Nernst equation for the oxygen concentration cell [20].

X-ray absorption spectra of powder samples were conducted on the beamline BL16A1 at the NSRRC in Taiwan. The electron storage ring was operated with an energy of 1.5 GeV and a current of 300 mA. A Si (111) double-crystal monochromator (DCM) was used for selection energy with a resolution of $1.5–2.1 \times 10^{-4}$. The monochromatized beam was then focused by a bent toroidal Glidcop mirror at 11.7 m and reached to the sample position at 18.20 m. That is a bend-magnet soft X-ray beamline, which provides good monochromatized photon beams with energies from 2 to 8 keV, that covers the *K*-edges of elements from P to Ni and *L*-edges of elements from Zr to Hf [21]. A Ti metal foil was used for the energy calibration. Ti *K*-edge spectrum was recorded under a transmission mode and detected by a gas ionization chamber. The intensity ratio of the low energy edge to the white light should be higher than 10 to ensure the quality of the spectrum. Ti *K*-edge data were collected from 4905 eV, which is below the edge (4966 eV), to 5115 eV, which is above the edge. Ti_2O_3 and TiO_2 (anatase) were used as reference standards to estimate the valence of the Ti atom in the YLT-2L samples.

Table 1
Amount of flux addition, preparation temperatures and the relative densities (including the standard deviation in the bracket) of the Y3LT samples.

x	Flux (wt.%)	Temperature (°C)	Relative density (%)
0	0	1600	94.3 (2)
0.040	0.31	1350	98.6 (3)
0.050	0.39	1350	97.7 (2)
0.070	0.55	1300	98.9 (3)
0.090	0.71	1300	97.4 (3)
0.100	0.79	1300	99.5 (5)
0.110	0.87	1300	99.4 (3)

3. Results and discussion

In our previous report, a series of $(Y_{2-x}Li_x)Ti_2O_{7-x}$ with $x = 0.040–0.110$ was prepared by adding $2x$ moles of the self-flux, $LiO_{0.5}$, into the parent compound. The sample is abbreviated as YLT-2L. YLT was the formula of the samples and 2L meant $2x$ moles of the $LiO_{0.5}$ flux co-existence with YLT. A solid state reaction method with a sintering temperature of 1150 °C was used to prepare them. The addition of the $LiO_{0.5}$ indeed lowered the preparation temperature for several hundred degree Celsius and increased the relative density of the samples to higher than 90(1)% [19]. All of them had pyrochlore phase. In this report, in order to have denser samples with higher relative density for the electrical conductivity measurement, sintering temperature was raised to at least 1300 °C. Table 1 lists the preparation temperatures and their relative densities for all the samples. In order to prepare dense $Y_2Ti_2O_7$, which has no flux addition, 1600 °C is required and its relative density is still lower than the rest of the samples which is only 94.3(2)%. For the $x = 0.040–0.060$, they were prepared at 1350 °C. The amount of flux addition was less than 0.50 wt.%, which is too little to effectively lower the sintering temperature. For $x \geq 0.070$, more $LiO_{0.5}$ was added so that the preparation temperature was further lowered to 1300 °C. All of the YLT-2L samples had relative densities higher than 97%.

Morphology of the $Y_2Ti_2O_7$ and a YLT-2L with $x = 0.070$ are shown in Fig. 1. SEM images were taken on the cross sectional area of the bulk sample. Their preparation temperatures were 1600 and 1300 °C, respectively. Both samples have grain size in the μm range. Empty holes as long as 1–5 μm appeared in the $Y_2Ti_2O_7$ sample, which had a relative density of 94.3(2)% listed in Table 1. On the other hand, relative densities of the YLT-2L samples were all over 97.2(6)%. Although $Y_2Ti_2O_7$ was prepared at 1600 °C, it had no flux addition, its relative density was smaller than the sample with an x of 0.070 prepared at 1300 °C with the addition of 0.55 wt.% of $LiO_{0.5}$. In Fig. 1, from the SEM images, grain boundary of the $Y_2Ti_2O_7$ is clearly seen, but for the YLT-2L sample, grains are partially melted together. The difference in preparation temperature between these two samples is 300 °C. The former was prepared at a higher temperature and is less dense than the latter. A small amount of flux indeed enhanced the relative density of these oxides.

Typical impedance Cole–Cole plots (Nyquist diagrams) for the YLT-2L samples were measured in the ambient pressure by a 2-probe configuration, Pt|YLT-2L|Pt. The impedance range corresponding to the grain, grain boundary, total and electrode resistances in the Cole–Cole plot is shown in Fig. 2. The Cole–Cole plot was taken from the frequency range from 1 M to 0.01 Hz. Two partially overlapping semicircles and a tail are observed. The one in the higher frequency range (on the left-hand side) is caused by the grain; the middle semicircle is attributed from the grain boundary and the last part (on the right-hand side) is from the electrode [22]. The grain and grain boundary contributions to the conducting process can be easily separated by using an appropriate equivalent circuit model [23]. One example for a sample with $x = 0.070$ is presented in Fig. 3. In our sample measurement, the frequency range is set in the range from 1 M to 1 Hz so that the contribution from the electrode in the small frequency range is not observed. At lower

Please cite this article as: L.C. Wen, et al., Solid State Ionics (2013), http://dx.doi.org/10.1016/j.ssi.2013.09.034

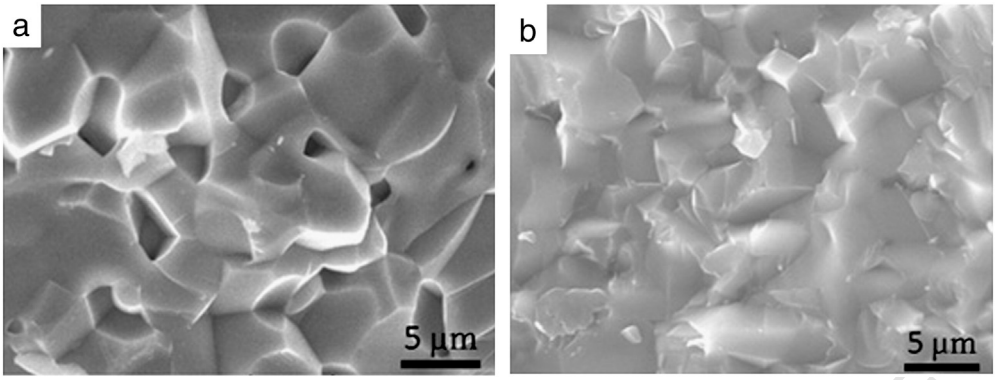

Q2 **Fig. 1.** SEM images of (a) the $Y_2Ti_2O_7$ and (b) a Y3LT with $x = 0.070$.

temperatures, two semicircles were observed. The impedance data were calculated by an equivalent circuit model with a series connection form $(R_g//C_g)(R_{gb}//C_{gb})$ shown in Fig. 3(a), where the symbols, 'g' and 'gb', represent the grain and grain boundary, respectively. These two contributions are in series [24]. The symbols of R and C in parallel represent the corresponding resistance and the universal capacitance in each contribution [25]. In Fig. 3(a), the grain resistance (R_g) is in the higher frequency semicircle and the grain boundary resistance (R_{gb}) is in the lower frequency one. The total impedance is counted from 0 to the end of the grain boundary semicircle. The total electrical conductivity, σ (total) is smaller than the sum of the σ (g) and σ (gb) due to the overlapping of these two semicircles. At higher temperatures, the Cole–Cole plot shifts toward higher frequencies. That is presumed due to the higher oxide ion conductivity of the target compound in this study [26,27]. Only the grain boundary semicircle was observed. Equivalent circuit model is changed to $R_g(R_{gb}//C_{gb})$ shown in Fig. 3(b). These two equivalent circuit models are employed to calculate the EIS results for all the samples.

The grain, grain boundary and total electrical conductivity at 600 °C as a function of the substitution amount of x for the YLT-2L and $Y_2Ti_2O_7$ samples are shown in Fig. 4. The decreasing order of these different conductivities is σ (gb) > σ (g) > σ (total) found for each sample. The shape of the curves for the σ (g) and the σ (total) is similar. The contribution to the σ (total) is mainly from the grain conductivity. An optimal value is found for the sample with $x = 0.070$. The σ (gb) is larger than the σ (g) that is probably related to the volume fractions between these two. In Fig. 1, SEM images show that the volume fraction of all the grains is bigger than that of the grain boundaries. As a result, grain boundary has smaller resistance so that the σ (gb) is larger than the σ (g). Adding flux into YLT-2L increases the grain size and lowers the melting point. Grain boundary becomes smeared, as shown in Fig. 1(b). That is helpful for the increase of the σ (gb). As a consequence, σ (gb) increases rapidly with increasing x till $x \leq 0.050$, which has less than 0.39 wt.% of flux addition. For the samples with $x \geq 0.50$, they contain more than 0.39 wt.% of flux, σ (gb) is slightly lowered with increasing the amount of flux. An optimal amount of flux (0.39 wt.%) in the YLT-2L samples was observed. Although more flux addition is still an advantage for the grain growth, they would probably accumulate in the grain boundaries and hinder the ionic transportation so that σ (gb) does not increase further [28,29]. A similar effect was also reported by Zhang et al. They used 0.5 at.% of $FeO_{1.5}$ as flux to prepare $Ce_{0.9}Gd_{0.1}O_{2-\delta}$. Both relative density and grain size were increased and the volume fraction of the grain boundary was decreased. They also found that σ (gb) is larger than σ (g) [30].

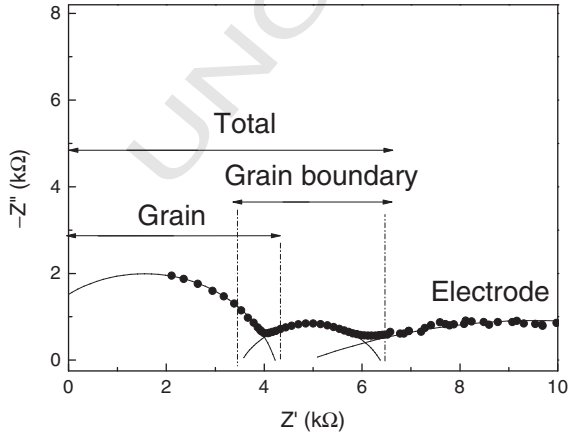

Fig. 2. The ranges corresponding to the grain, grain boundary and total impedances were marked for a YLT-2L with $x = 0.070$ measured at 500 °C by the frequencies between 0.01 and 1 MHz.

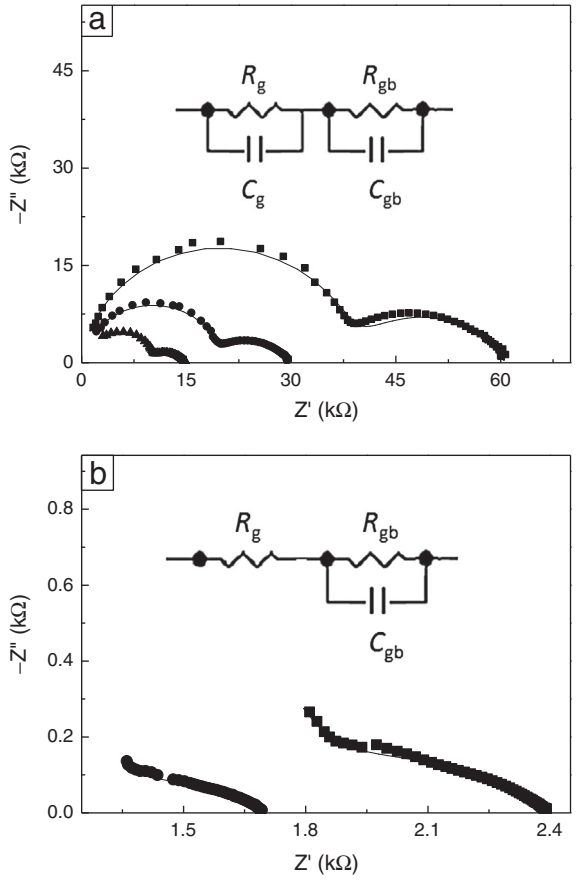

Fig. 3. Complex impedance plots obtained at (a) (■) 436, (●) 468 and (▲) 500 °C and (b) (■) 625 and (●) 661 °C for a Y3LT sample with $x = 0.070$. The equivalent circuit models are shown in the figures.

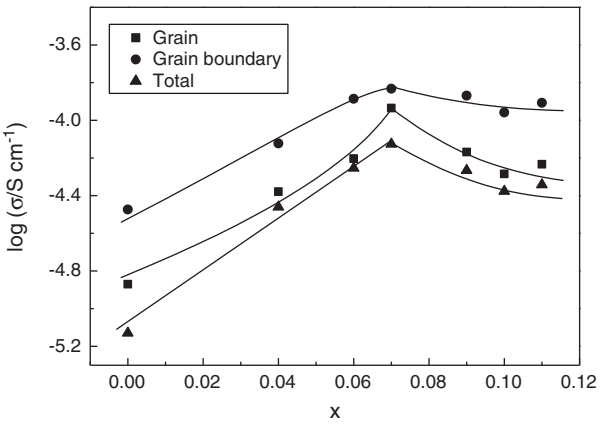

Fig. 4. The (■) grain, (●) grain boundary and (▲) total electrical conductivity at 600 °C as a function of the substitution amount of *x* for the Y3LT.

$Y_2Ti_2O_7$ is the only sample without Li^+ ion doping. No oxygen vacancies were created to increase the electrical conductivity so that it has the smallest values, including the σ (g), σ (gb) and σ (total). In addition, there is no sintering aid ($LiO_{0.5}$) addition in synthesizing the $Y_2Ti_2O_7$. The relative density of it is smaller than the rest of the samples so that it has the smallest σ (gb). A slightly porous sample with a relative density of 94% and clear grain boundaries in the $Y_2Ti_2O_7$ shown in Fig. 1(a) leads to the lower σ (gb) [31,32].

For the curve of the σ (g), conductivity increases rapidly by increasing the amount of substitution till $x \le 0.070$. The chemical formula of these samples is $(Y_{2-x}Li_x)Ti_2O_{7-x}$. This increases the amount of substitution and creates more oxygen vacancies, which is an advantage for the oxygen ion conduction. The migration distance is shortened due to the shrinking of the unit cell by introducing the smaller Li^+ ions into the bigger Y-site so that electrical conductivity for the YLT-2L increases by increasing *x* to $x = 0.070$. For $x > 0.070$, although the amount of oxygen vacancies is still increased, the unit cell becomes even smaller with further increase of the *x* due to the size of the Li^+ ion, which is smaller than the Y^{3+} ion [33]. Shrinking the unit cell volume leads to the shortening of the bond distance between cations and anions that increases the binding force between ions. That would increase the difficulty for the oxygen ion migration and cause the decrease of the electrical conductivity. Thus, the σ (g) decreases by increasing *x* when $x > 0.070$. A similar trend of the σ (total) dependence on the *x* is also observed and plotted in Fig. 4.

Comparing the conductivity for the whole series, the YLT-2L with $x = 0.070$ has the highest σ (total). There are many factors that possibly influence the total electrical conductivity, such as, substitution amount (*x*), oxygen vacancy concentration, unit cell size, bond distance, interaction between cation and anion, flux amount, grain size, relative density, etc. Some of them are positive and the rest are negative. It is difficult to find a specific reason to explain the overall results. An optimal σ (total) is observed in a YLT-2L with $x = 0.070$, which was 7.49×10^{-5} S·cm^{-1} at 600 °C. When the temperature is raised to 700 °C, the σ (g) does not appear in the Cole–Cole plot and only σ (gb) and σ (total) can be extracted. They are 6.83×10^{-4} and 2.90×10^{-4} S·cm^{-1}, respectively. Electrical conductivity of the YLT-2L with $x = 0.070$ at 700 °C is larger than that of the $Y_2Ti_2O_7$ reported [17,18,34]. All of them prepared $Y_2Ti_2O_7$ at 1600 °C, and electrical conductivity was in the range of 1–2.3×10^{-4} S·cm^{-1}. Norberg et al. prepared $Y_2Ti_2O_7$ at 1550 °C, and the relative density was only 65–70%. The bulk ionic and grain boundary conductivities were only 1.26×10^{-6} and 1.51×10^{-6} S·cm^{-1}, respectively [35]. We prepared $(Y_{2-x}Li_x)Ti_2O_{7-x}$ samples with $x \ge 0.070$ at 1300 °C with the co-existence of flux, and electrical conductivity was higher than their results. Not only was the preparation temperature lowered to 300 °C, but the electrical conductivity was also enhanced. Substitution and the addition of flux had a great advantage in synthesizing these titanates.

The unit cell size is mentioned in our previous report [36] to be one important factor in governing the electrical conductivity of the ionic conductors. The bond distance is directly related to the unit cell size. Thus, Fig. 5 plots the σ (g) and σ (total) at 600 °C with respect to the bond distance of the A–O (1), where A is the Y-site and O (1) is one of the oxygen sites, 48*f*. In this figure, no σ (gb) is shown because the grain boundary conductivity is not related to the unit cell size or the bond distance. The shape of both curves is similar. The influence of the σ (g) to the σ (total) is clearly seen. Both curves show an optimal value near 2.491 Å for the A–O (1) bond distance. This sample has a unit cell *a*-axis of 10.1028(4) Å. Wuensch et al. prepared two series of samples, $Y_2(Sn_yTi_{1-y})_2O_7$ and $Gd_2(Sn_yTi_{1-y})_2O_7$. They found an optimal conductivity for each series with $y = 0.4$ measured at 1000 °C. Due to the size difference between Y and Gd, the unit cell size of these two series is different. As a result, the bond distance of the Y–O (1) is not the same as that of the Gd–O (1) for the sample having the optimal conductivities [37]. Therefore, bond distance is not a universal parameter to find the highest electrical conductivity of these titanates. Liu et al. prepared two series of samples with the formulas as $Sm(Yb_{1-x}Mg_x)Zr_2O_{7-x/2}$ $(0 \le x \le 0.15)$ and $(Sm_{2-x}La_x)Zr_2O_7$ $(0 \le x \le 1)$. They found that optimal conductivity in the former was the one with $x = 0.15$ and the latter was $x = 0$. At 700 °C, conductivities were 2.24×10^{-4} and 2.51×10^{-4} S·cm^{-1}, respectively [38]. The former has Yb and Mg co-doping and the latter has no dopant. The samples having the optimal conductivities have different unit cell *a*-axis, 10.450 and 10.595 Å, respectively so that the bond distance is not the same either. Marrocchelli et al., using ab initio electronic calculations on the YSZ and ScSZ, found a maximum conductivity for each series [11]. By reducing the doping cation size, conductivity increased. Therefore, different dopants, either at the A-site or the B-site create optimal conductivity with different substituting amounts, unit cell sizes and bond distances. These parameters cannot be used to determine the optimal electrical conductivity for different series.

The grain, grain boundary and total conductivity dependence on the temperature of a YLT-2L with $x = 0.040$ are plotted in Fig. 6. All the samples have similar results. Only one of them is shown to make the figure easily viewed. Two straight lines were fitted for the σ (gb). The lower temperature (LT) region is 500–600 °C and the higher temperature (HT) range is 600–700 °C. The YLT-2L with $x = 0.040$ has the largest difference of these two slopes that is why it was chosen for presentation. However, only one slope was fitted for the σ (g) and σ (total). Both σ (g) and σ (total) obey the Arrhenius equation well. The correlation values (R^2) found for all the samples are in the range of 0.9978–0.9994, they are quite close to 1 so that the ionic diffusion is an activated behavior. The E_a (gb in HT), E_a (gb in LT), E_a (g) and E_a

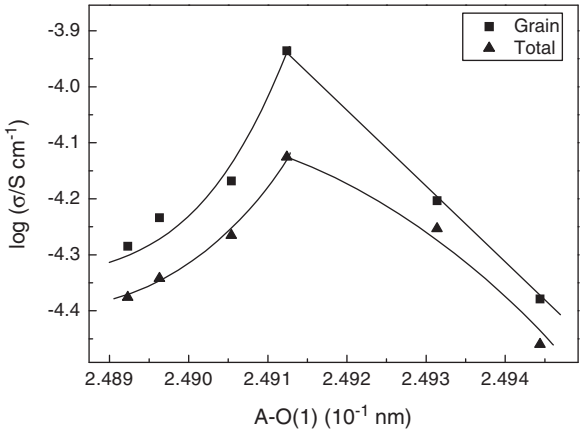

Fig. 5. The (■) grain and (▲) total electrical conductivity at 600 °C as a function of the A–O(1) bond distance for the Y3LT.

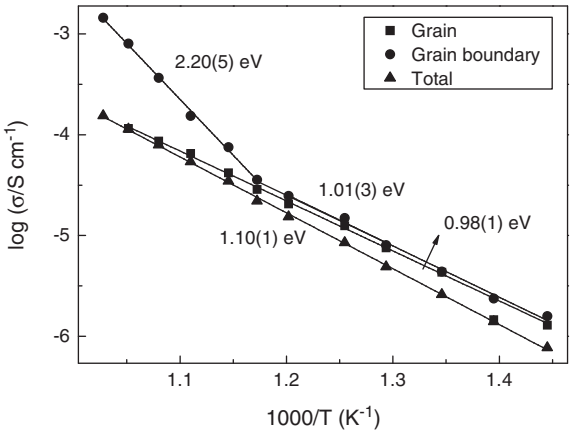

Fig. 6. Temperature dependence of the (■) σ (grain), (●) σ (grain boundary) and (▲) σ (total) of a Y3LT with $x = 0.040$.

(total) are 2.20(5), 1.10(3), 0.98(1) and 1.01(1) eV for this sample. The E_a (gb in HT) is relatively high. The relation of the activation energy (E_a) versus x is shown in Fig. 7. In Fig. 7(a), both grain boundary activation energies in the HT and LT are shown. The E_a (gb in HT) is larger than the E_a (gb in LT) for each sample. At a higher temperature, the conductivity increases and the possibility of the oxygen ion to cross over the grain boundary increases so that the E_a (gb in HT) is enhanced. At lower temperature, the ionic diffusion rate is limited. The chance to cross over the grain boundary is also limited. Therefore, the E_a (gb in LT) is smaller and the variation of the E_a (gb in HT) between samples is small. The amount of flux that remains in the grain boundary has a greater effect on the E_a (gb in HT) than the E_a (gb in LT). For the sample with $x = 0.070$, it has the smallest E_a (gb in HT). There are several factors that possibly influence the value of the E_a at grain boundary, such as, particle size, relative density and the amount of flux addition [30]. It seems that the $x = 0.070$ sample has the optimal combination. For the $Y_2Ti_2O_7$, it was prepared at 1600 °C but the sample with $x = 0.040$ was prepared at 1350 °C. Different preparation temperatures probably cause the difference of the E_a (gb in HT). The apparently high E_a (gb in HT) for the sample with $x = 0.040$ is probably due to the amount of flux addition that is only 0.31%. A little amount of flux leads to a smaller grain size and a higher grain boundary density. For the samples with $x < 0.070$, their grain size becomes bigger gradually, which decreases the density of the grain boundary and enhances the conductivity contributed by the grain boundary. For the $x > 0.070$ samples, although the grain size keeps growing, the sintering aid would accumulate at the grain boundary region. This also increases the difficulty for the oxygen ion migration [39]. E_a (gb) for the $x > 0.070$ is not as large as those samples with a smaller amount of substitution which is due to the larger grain size and lower grain boundary density, although there may be too much flux remaining in the grain boundary to hinder the electrical conductivity.

In Fig. 7(b), E_a (g) and E_a (total) are plotted. The sample with $x = 0.070$ has the smallest E_a. The factors governing the E_a (g) include the amount of substitution, unit cell size, bond distance between cation and anion and amount of vacancies. It seems that the sample with $x = 0.070$ has the optimal conditions. E_a (total) for our sample, a YLT-2L with $x = 0.070$, $Y_2Ti_2O_7$ and the literature reports are 0.99(1), 1.09(1), 0.86 [17] and 1 eV [34] in which, YLT-2L with $x = 0.070$ was prepared at 1300 °C and the rest of them were prepared at 1600 °C. E_a (total) found for the titanates with a pyrochlore structure is generally near 1 eV.

The effect of the oxygen partial pressure on the electrical conductivity for a YLT-2L with $x = 0.070$ measured at 600 and 700 °C is shown in Fig. 8. The electrical conductivities do not change with respect to the oxygen partial pressures varied from 10% to 100%. Average electrical conductivities measured at 700 °C with different oxygen partial pressures for each of the $(Y_{2-x}Li_x)Ti_2O_{7-x}$ with $x = 0$–0.110 are listed in Table 2. Standard deviation shows the σ obtained under different partial pressures. The largest standard deviation is found in the $x = 0.100$ sample, which is 1.76 ± 0.08 or 1.76 ± 5%. The smallest one is the $x = 0.070$ sample, which is 4.41 ± 0.01, or less than 1% change. In summary, σ (total) does not change under the oxygen partial pressure variations from 10 to 100% for each sample.

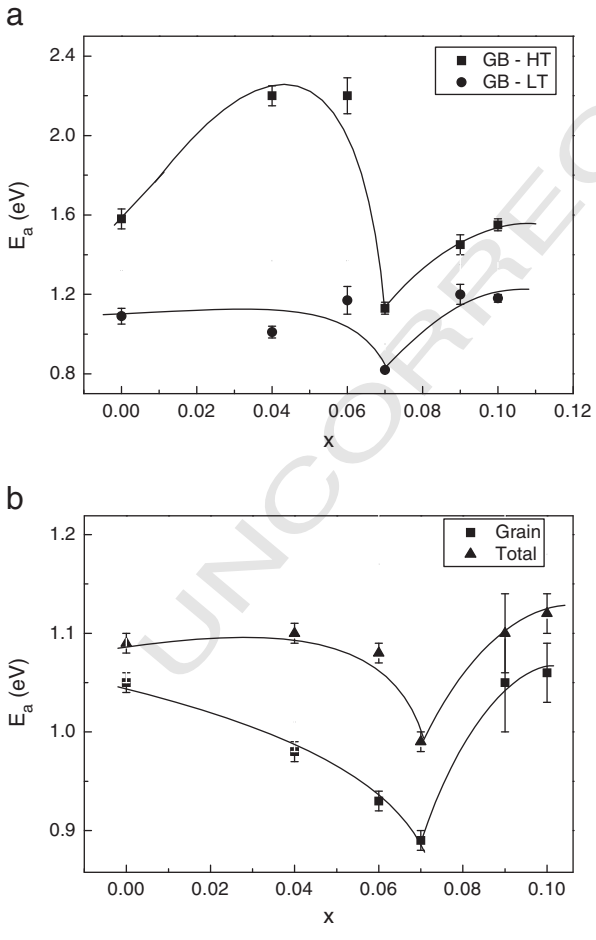

Fig. 7. Activation energies of the (a) (■) grain boundary in 600–700 °C and (●) grain boundary in 500–600 °C; (b) the (■) grain and (▲) total as a function of x for the YLT-2L system.

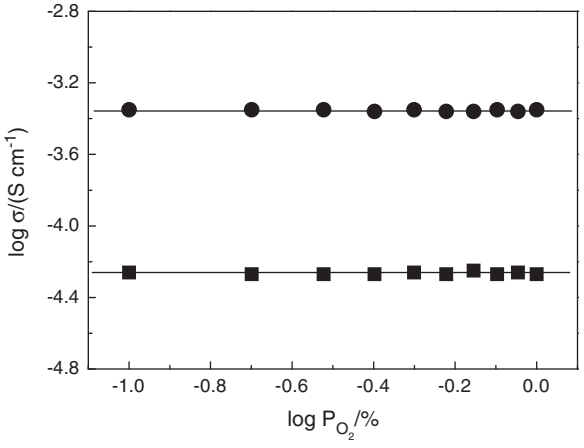

Fig. 8. Total electrical conductivities as a function of the oxygen partial pressures at (■) 600 and (●) 700 °C for a Y3LT with $x = 0.070$.

Table 2
Average electrical conductivities measured at 700 °C under different oxygen partial pressures and the transference numbers measured at different temperatures for all the Y3LT samples.

x	Avg. σ_{700} (10^{-4} S·cm^{-1})[a]	t_{i500}	t_{i600}	t_{i700}
0	0.326 (6)	1.00 (3)	0.96 (1)	0.91 (1)
0.040	1.55 (4)	1.00 (2)	0.96 (2)	0.91 (2)
0.050	1.89 (5)	1.00 (1)	0.96 (1)	0.92 (1)
0.070	2.90 (3)	1.00 (3)	0.98 (1)	0.91 (2)
0.090	2.05 (2)	1.00 (2)	0.95 (3)	0.89 (4)
0.100	1.69 (8)	1.00 (1)	0.97 (1)	0.92 (1)
0.110	1.88 (2)	1.00 (3)	0.95 (3)	0.88 (4)
Average t_i		1.00 (2)	0.96 (1)	0.90 (1)

[a] Standard deviation is calculated from the σ_{700} obtained under different oxygen partial pressures.

In order to understand the contribution from electronic conduction in the operating temperature, EMF (electromotive force) was measured at 500, 600 and 700 °C. A gas mixture of oxygen and argon was introduced to one side of the oxygen concentration cell, and the other side was exposed in ambient air as a reference. Theoretical potential is calculated by the Nernst equation for the oxygen concentration cell [20]. Table 2 lists the transference numbers (t_i) for all the samples at different temperatures. They are 1.00(2), 0.96(2) and 0.90(3). Ionic transference numbers of these materials decreased gradually by increasing the measuring temperature. At 600 and 700 °C, the electronic transference numbers (t_e) are 0.04 and 0.10, respectively. The EMF measurement on the $Y_2Ti_2O_7$ by Kobayashi et al. also found that the transference number decreased with increasing the measuring temperature [18]. The results show that the fraction of the electronic contribution increases with an increasing temperature. Hence, the E_a (ionic) is smaller than the E_a (electronic) so that the increasing rate of the electronic conduction is more apparent at a higher temperature. The total activation energies for these YLT-2L samples are in the range of 0.99(1) to 1.12(2) eV. If the YLT-2L and $Y_2Ti_2O_7$ samples have the electronic semiconducting behavior, we deduce that they have an energy gap of ~3 eV. Comparing with the related compounds, such as TiO_2-rutile and anatase, which have gaps of 3.03 eV and 3.20 eV, respectively [40], Bi_2O_3 and $BaTiO_3$ have gaps of 2.8 eV [41] and 3.3 eV [42], respectively.

Table 2 also shows that t_i and t_e do not depend on the amount of the dopant and the flux addition. Therefore, the average value and standard deviation among the samples are calculated for all of them at each measuring temperature and listed on the last line of Table 2. In Fig. 9, the average t_i of the YLT-2L and $Y_2Ti_2O_7$ with respect to the measuring temperatures is plotted. At 500 °C, all the YLT-2L and $Y_2Ti_2O_7$ have a pure ionic conduction. No electronic contribution is found.

The existence of the electronic conductivity implies that Ti atoms are in the mixed valence states. A major contribution of the electronic conductivity is probably coming from the mixed-valence of the Ti-atom. $Y_2Ti_2O_7$ is well known as a mixed ionic–electronic conductor [17,18,34]. The ionic transference number of the $Y_2Ti_2O_7$ had been reported by Kobayashi et al. Their results showed that the amount of Ti^{4+} also decreased by increasing the measuring temperature [34]. The Ti *K*-edge XANES spectra for the three YLT-2L samples with $x =$ 0.040, 0.080, and 0.110 and two references, Ti_2O_3 and TiO_2 (anatase) are shown in Fig. 10. The curve shape for all the samples and the TiO_2-anatase are similar. Clearly, the shoulder of the Ti_2O_3 is located at the lower energy side, an indication of the lower valence. The photon energy at the absorption edge maximum can be used for the valence comparison. Energies corresponding to the samples and anatase are 4986.0 and 4987.0 eV, respectively. All the YLT-2L samples had the same results. The average valence of the Ti atoms did not vary with the amount of Li ion substitution and the flux addition. The valence of the Ti atoms was close to 4 but slightly less than 4. Small amount of Ti atoms was not in the 4+ valence state.

4. Conclusions

Preparation temperature is lowered for more than 250 °C by the addition of $LiO_{0.5}$ self-flux into the $(Y_{2-x}Li_x)Ti_2O_{7-x}$ system. Relative density of the samples is about fully dense. By the substitution of the Li ions into $Y_2Ti_2O_7$, oxygen vacancies were created in the $(Y_{2-x}Li_x)Ti_2O_{7-x}$ system, which was helpful for the ionic conduction. As a result, although there was flux co-existence in the YLT-2L samples, electrical conductivities of them are still higher or comparable to the $Y_2Ti_2O_7$ found in the literature reports. The sample with $x = 0.070$ has the highest conductivity, 2.90×10^{-4} S·cm^{-1} at 700 °C and the lowest activation energy, 0.99 eV. At 500 °C, ionic transference numbers found for all the samples are 1.00 and no electronic conductivity is observed. If one is interested in using these titanates as an electrolyte material, it is suggested to use it under 500 °C. A small amount of the Ti atom is in the Ti^{3+} state, which might increase the electronic conduction at higher temperature.

Acknowledgment

This work is supported by the Institute of Nuclear Energy Research, Atomic Energy Council of Taiwan under contract numbers 1012001INER039 and 1022001INER032.

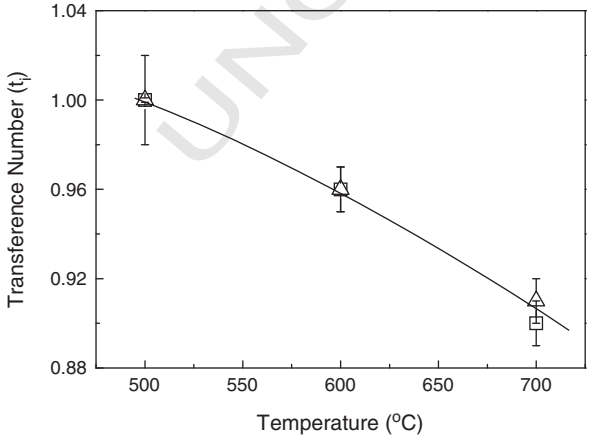

Fig. 9. Average ionic transference numbers and the standard deviations as a function of the temperatures for the (□) Y3LT with $x = 0.040$–0.110 and (Δ) $Y_2Ti_2O_7$.

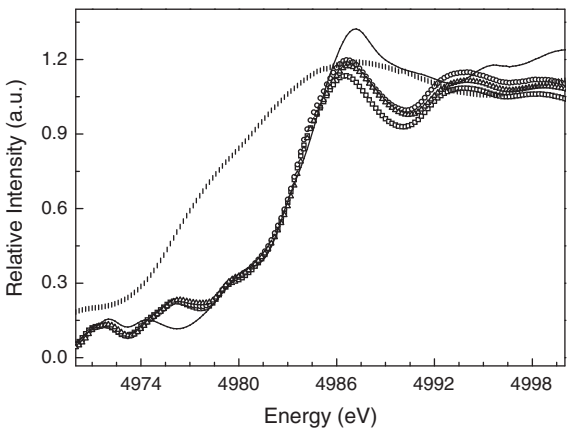

Fig. 10. Normalized Ti *K*-edge XANES spectra of (|) Ti2O3, (−) TiO2-anatase, and YLT-2L with $x =$ (□) 0.040, (○) 0.080 and (Δ) 0.110.

Please cite this article as: L.C. Wen, et al., Solid State Ionics (2013), http://dx.doi.org/10.1016/j.ssi.2013.09.034

References

[1] C. Lara, M.J. Pascual, A. Duran, J. Glass Sci. Technol. B 48 (2007) 218–224.
[2] A. Lashtabeg, S.J. Skinner, J. Mater. Chem. 16 (2006) 3161–3170.
[3] Z. Wang, K. Sun, S. Shen, N. Zhang, J. Qiao, P. Xu, J. Membr. Sci. 320 (2008) 500–504.
[4] Y. Li, Y. Xie, J. Gong, Y. Chen, Z. Zhang, Mater. Sci. Eng. B 86 (2001) 119–122.
[5] B. Gharbage, M. Henault, T. Pagnier, A. Hammou, Mater. Res. Bull. 26 (1991) 1001–1007.
[6] N. Miura, H. Jin, R. Wama, S. Nakakubo, P. Elumalai, V.V. Plashnitsa, Sensors Actuators B 152 (2011) 261–266.
[7] T.H. Etsell, S.N. Flengas, Chem. Rev. 70 (1970) 339–376.
[8] B.J. Kennedy, B.A. Hunter, C.J. Howard, J. Solid State Chem. 130 (1997) 58–65.
[9] Y.H. Lee, H.S. Sheu, J.P. Deng, H.-C.I. Kao, J. Alloys Compd. 487 (2009) 595–598.
[10] C.W. Chiu, Y.H. Lee, H.S. Sheu, H.-C.I. Kao, J. Chin. Chem. Soc. 57 (2010) 925–931.
[11] Y.H. Lee, H.S. Sheu, H.-C.I. Kao, Mater. Chem. Phys. 124 (2010) 145–149.
[12] H. Yamamura, H. Nishino, K. Kakinuma, K. Nomura, J. Solid State Chem. 158 (2003) 359–365.
[13] T. Shimura, M. Komori, H. Iwahara, Solid State Ionics 86–88 (1996) 685–689.
[14] A.V. Shlyakhtina, L.G. Shcherbakova, A.V. Knotko, A.V. Steblevskii, J. Solid State Electrochem. 8 (2004) 661–667.
[15] V.V. Ivanov, V.R. Khrustov, Yu.A. Kotov, A.I. Medvedev, A.M. Murzakaev, S.N. Shkerin, A.V. Nikonov, J. Eur. Ceram. Soc. 27 (2007) 1041–1046.
[16] J.S. Lee, K.H. Choi, M.W. Park, Y.G. Choi, J.H. Mun, J. Alloys Compd. 474 (2009) 219–222.
[17] S. Yamaguchi, K. Kobayashi, K. Abe, S. Yamazaki, Y. Iguchi, Solid State Ionics 113 (1998) 393–402.
[18] K. Kobayashi, M. Mukaida, T. Tsunoda, Y. Imai, Solid State Ionics 154–155 (2002) 101–107.
[19] L.C. Wen, H.Y. Hsieh, Y.H. Lee, S.C. Chang, H.-C.I. Kao, H.S. Sheu, I.-N. Lin, J.C. Chang, M.C. Lee, Y.S. Lee, Solid State Ionics 206 (2012) 39–44.
[20] A.R. West, Basic Solid State Chemistry, 2nd ed. Wiley, New York, 1999. 351–361.
[21] T.E. Dann, S.C. Chung, L.J. Huang, J.M. Juang, C.I. Chen, K.L. Tsang, J. Synchrotron Radiat. 5 (1998) 664–666.
[22] N.J. Hoboken, Impedance Spectroscopy: Theory, Experiment, and Applications, 2nd ed. Wiley & Sons, New Jersey, 2005. 230.
[23] M.H. Abdullah, A.N. Yusoff, J. Mater. Sci. 32 (1997) 5817–5823.
[24] Z.G. Liu, J.H. Ouyang, Y. Zhou, X.L. Xia, J. Power Sources 195 (2010) 3261–3265.
[25] J.A. Díaz-Guillén, M.R. Díaz-Guillén, K.P. Padmasree, A.F. Fuentes, J. Santamaría, C. León, Solid State Ionics 179 (2008) 2160–2164.
[26] J. Plocharski, W. Wieczorek, Solid State Ionics 28–30 (1988) 979–982.
[27] K.S. Sibi, A.N. Radhakrishnan, M. Deepa, P.P. Rao, P. Koshy, Solid State Ionics 180 (2009) 1164–1172.
[28] J. Ayawanna, D. Wattanasiriwech, S. Wattanasiriwech, P. Aungkavattana, Solid State Ionics 180 (2009) 1388–1394.
[29] T.S. Zhang, J. Ma, Y.J. Leng, Z.M. He, J. Cryst. Growth 274 (2005) 603–611.
[30] T.S. Zhang, J. Ma, L.H. Luo, S.H. Chan, J. Alloys Compd. 422 (2006) 46–52.
[31] C. Wagner, Naturwissenschaften 31 (1943) 265–268.
[32] S. Hull, Rev. Prog. Phys. 67 (2004) 1233–1314.
[33] R.D. Shannon, Acta Crystallogr. A 32 (1976) 751–767.
[34] K. Uematsu, J.K. Shinozaki, O. Sakurai, N. Mizutani, M. Kato, J. Am. Ceram. Soc. 62 (1979) 219–224.
[35] S.T. Norberg, S. Hull, S.G. Eriksson, I. Ahmed, F. Kinyanjui, J.J. Biendicho, Chem. Mater. 24 (2012) 4294–4300.
[36] W.P. Su, Y.H. Lee, C.T. Hsieh, H.S. Sheu, J.F. Lee, Y.P. Chiang, H.-C.I. Kao, J. Chin. Chem. Soc. 56 (2009) 1112–1117.
[37] B.J. Wuensch, K.W. Eberman, C. Heremans, E.M. Ku, P. Onnerud, E.M.E. Yeo, S.M. Haile, J.K. Stalick, J.D. Jorgensen, Solid State Ionics 129 (2000) 111–133.
[38] Z.G. Liu, X.Z. Xiong, J.H. Ouyang, J. Xiang, Electrochim. Acta 56 (2011) 2837–2841.
[39] T.S. Zhang, J. Ma, L.B. Kong, S.H. Chan, P. Hing, J.A. Kilner, Solid State Ionics 167 (2004) 203–207.
[40] K. Yoshida, J. Yamasaki, N. Tanaka, Appl. Phys. Lett. 84 (2004) 2542–2544.
[41] N. Herron, J.C. Calabrese, W.E. Farneth, Y. Yang, Science 259 (1993) 1426–1428.
[42] S.H. Wemple, M. Didomenico Jr., I. Camlibel, J. Phys. Chem. Solids 29 (1968) 797–1803.

Please cite this article as: L.C. Wen, et al., Solid State Ionics (2013), http://dx.doi.org/10.1016/j.ssi.2013.09.034